Aust. J. Phys., 1990, **43**, 45–64

Ion Densities in Low Temperature Nitrogen Plasmas

I. J. Donnelly and E. K. Rose

Australian Nuclear Science and Technology Organisation,
Lucas Heights Research Laboratories,
Private Mail Bag 1, Menai, N.S.W. 2234, Australia.

Abstract

A cross-section library for the electron ionisation of hydrogen and nitrogen molecules, atoms and ions has been assembled and used for the derivation of reaction rate coefficients assuming a Maxwellian distribution of electron energies. For fixed electron temperatures, the steady-state and time-dependent ionisation of nitrogen molecules have been calculated for conditions relevant to glow discharge plasmas in which the dominant recombination mechanism occurs via the plasma–wall interaction. The analysis shows that there is a threshold electron temperature below which there is no steady-state ionisation. For a small range of temperatures above this threshold there are two possible ionisation states, but at higher temperatures only the more highly ionised state persists. The dependence of the ratio of N^+ to N_2^+ ions on filling pressure, confinement time and electron density is also discussed.

1. Introduction

Low temperature plasmas which are not in thermodynamic equilibrium are commonly applied to the processing of materials in fields such as plasma etching (Coburn and Winters 1983), sputter deposition (Thornton 1982), ion plating and ion nitriding (Korhonen *et al.* 1988), plasma-enhanced chemical vapour deposition (Hess 1986) and plasma immersion ion implantation (Conrad *et al.* 1987; Tendys *et al.* 1988), henceforth called PI^3. The understanding of these processes depends in part on knowledge of plasma properties such as ion densities and electron temperature. The development of methods to calculate these parameters is clearly desirable and it has been receiving considerable attention.

In this paper we concentrate on the properties of the nitrogen plasmas being used at ANSTO for PI^3 (Tendys *et al.* 1988). These plasmas are generated by inductively coupling radio frequency power into nitrogen gas at filling pressures of a few mTorr. In PI^3, the plasma acts as a source of ions which are accelerated into a target that is at a large negative voltage (≈–50 kV) with respect to the plasma in which it is immersed. Prediction and optimisation of the dose and depth of implantation depend on knowledge of the number

0004-9506/90/010045$03.00

densities of the N_2^+ and N^+ ions in the plasma, and how they depend on parameters such as filling pressure and rf power.

Calculations of the ionisation of plasmas require electron–molecule and electron–atom cross sections. The ionisation cross sections are readily available for the atomic species (Lennon *et al.* 1986). However, there is a paucity of data for molecular cross sections, many of which are difficult to determine either experimentally or theoretically. We have assembled in the data library file EKR.ATMOLIB the relevant atomic and molecular ionisation, dissociation and recombination cross sections for hydrogen and nitrogen for electron energies in the range 1 eV to 1 keV. The hydrogen data are included for comparison with the nitrogen data, and also because it has application to ionisation processes in rotamak plasmas (Donnelly *et al.* 1987). The molecular reaction rate coefficients have been evaluated for electron temperatures in the range $1 \leq T_e \leq 50$ eV using the assumption that the electron energy distribution is Maxwellian. The atomic cross section and reaction rate coefficient data were taken from the compilation of Lennon *et al.* (1986).

In well confined, or medium to high density plasmas, the radiative and dielectronic electron–ion recombination rates are also needed to allow calculation of the densities of ionised states. Here we restrict our analysis to plasmas with electron density n_e (cm^{-3}), electron temperature T_e (eV) and particle confinement time τ (s) which satisfy $n_e \tau \ll 10^9 T_e^{3/2}$ cm^{-3} s, in which case the dominant recombination mechanism occurs via ion–wall contact, so that electron–ion recombination in the body of the plasma can be ignored.

The appropriate rate equations have been formulated and used to obtain the steady-state values and the evolution in time of the neutral and ionised population densities in low temperature ($T_e < 10$ eV) nitrogen plasmas at low filling pressures (below a few mTorr). Analytic and numerical solutions of the steady-state equations show that there is a threshold temperature below which there is no ionisation. For a small range of temperatures above this threshold there are two possible ionisation states, but at higher temperatures only the more highly ionised state exists. The threshold temperature decreases as the filling pressure or the confinement time increases.

2. The Plasma Model

The nitrogen plasmas used for the PI[3] experiments reported by Tendys *et al.* (1988) were generated in a spherical glass vessel of radius $R = 15$ cm by radio frequency fields ($\omega/2\pi = 13 \cdot 56$ MHz) excited by a pair of antenna coils external to the vessel. The neutral density n (cm^{-3}) was typically about 10^{14} cm^{-3} (≈3 mTorr filling pressure) and the electron densities were in the range 10^8–10^{10} cm^{-3}, depending on the input power. In these plasmas the electron scattering is dominated by collisions with neutrals and the electron mean free path is $\lambda_{en} \approx 10$ cm. As the electron mean free path is comparable with the vessel dimensions, the plasma density is fairly uniform apart from the sheath regions around the target and at the vessel walls. In this case the plasma confinement is determined by the collisionless ambipolar diffusion rate, with a confinement time τ of the order $R/3c_s$ where $c_s \approx 10^6 (T_e/A)^{1/2}$ $cm\,s^{-1}$ is the acoustic speed. For $t_e = 5$ eV and the ratio of ion mass to proton mass

$A = 28$, we find $\tau \approx 10\,\mu$s. In more recent PI^3 experiments the vessel is larger, so we take $\tau = 20\,\mu$s in the numerical work presented later.

A very large literature exists on the study of ionisation and transport processes in glow discharge plasmas which are generated by steady-state or rf electric fields. Over a wide range of filling pressures, electric field strengths E and rf frequencies, much of the plasma behaviour depends predominantly on the parameter E_e/n, where $E_e = \nu_{en} E/(\nu_{en}^2 + \omega^2)^{1/2}$ is the 'effective' electric field strength and ν_{en} ($\approx 2 \cdot 4 \times 10^{-7} n$ in nitrogen for $2 < T_e < 10$ eV) is the electron–neutral collision frequency (Ferreira and Loureiro 1989). The major difference between the plasmas analyses here and those more commonly considered arises from the long mean free paths and the small values of the parameter $n\tau$ associated with the PI^3 plasmas.

The parameter E_e/n is spatially non-uniform in the plasmas used by Tendys *et al.* (1988), but an estimate of the maximum value and the spatial variation is possible. Since $\omega \ll \omega_{pe}$ (the plasma frequency) and since $\omega \gg \nu_{en}$, penetration of the rf fields is determined by the collisionless skin depth $\delta = c/\omega_{pe} = 5 \cdot 4 \times 10^5 n_e^{-1/2}$ cm. For PI^3 plasmas with $n_e \approx 10^{10}$ cm^{-3}, $\delta \approx 5$ cm. The electric field is largest in the plasma regions nearest to the antenna coils, with a maximum value of about 1 V cm^{-1}, which gives $E_e/n \approx 3 \times 10^{-15}$ V cm^2. It is also worth noting that the rf electric field is predominantly parallel to the walls as it is in the azimuthal direction around the antenna coil axis which runs along a diameter of the vessel.

Evaluation of the electron reaction rate coefficients requires that the electron energy distribution function (EEDF) be known. An accurate calculation of the EEDF in an rf generated plasma is a very complex task (e.g. Ferreira and Loureiro 1989; Kushner 1983) which requires knowledge of the electron scattering and molecular excitation cross sections as well as the cross sections considered in this paper. It may also involve boundary conditions and the effects of secondary electrons emitted from cathodes and walls. For electron temperatures of 5 eV or less only the high energy tail of the EEDF (electron energy $u > 10$ eV) leads to dissociation and ionisation, and these inelastic events may lead to depletion of the EEDF in this region. However, an opposing effect is the increase in electron energy because of superelastic collisions with vibrationally excited molecules. The work of Ferreira and Loureiro (1989) shows that these two effects essentially balance for plasmas generated by an effective E_e/n of $\approx 3 \times 10^{-15}$ V cm^2, and the molecular ionisation rate coefficients derived using a Maxwellian EEDF and their calculated EEDF are in agreement to within a factor of $\approx 1 \cdot 5$. Since the ionisation and dissociation cross sections have a similar energy dependence, as can bee seen in Fig. 2*a* in Section 3, the relative values of derived reaction rate coefficients will not depend strongly on the variation of the EEDF from a Maxwellian provided that this variation is not extreme in the energy range $10 < u < 20$ eV. The results of Ferreira and Loureiro (1989) are not directly applicable to the PI^3 plasmas considered here because their calculations assumed no diffusion losses, whereas this loss rate is fairly high for the PI^3 plasmas, particularly for those electrons which have energies above the plasma–wall sheath potential. This will deplete the EEDF to some extent in the high energy region. The likely effects of this depletion on the results reported here is discussed later.

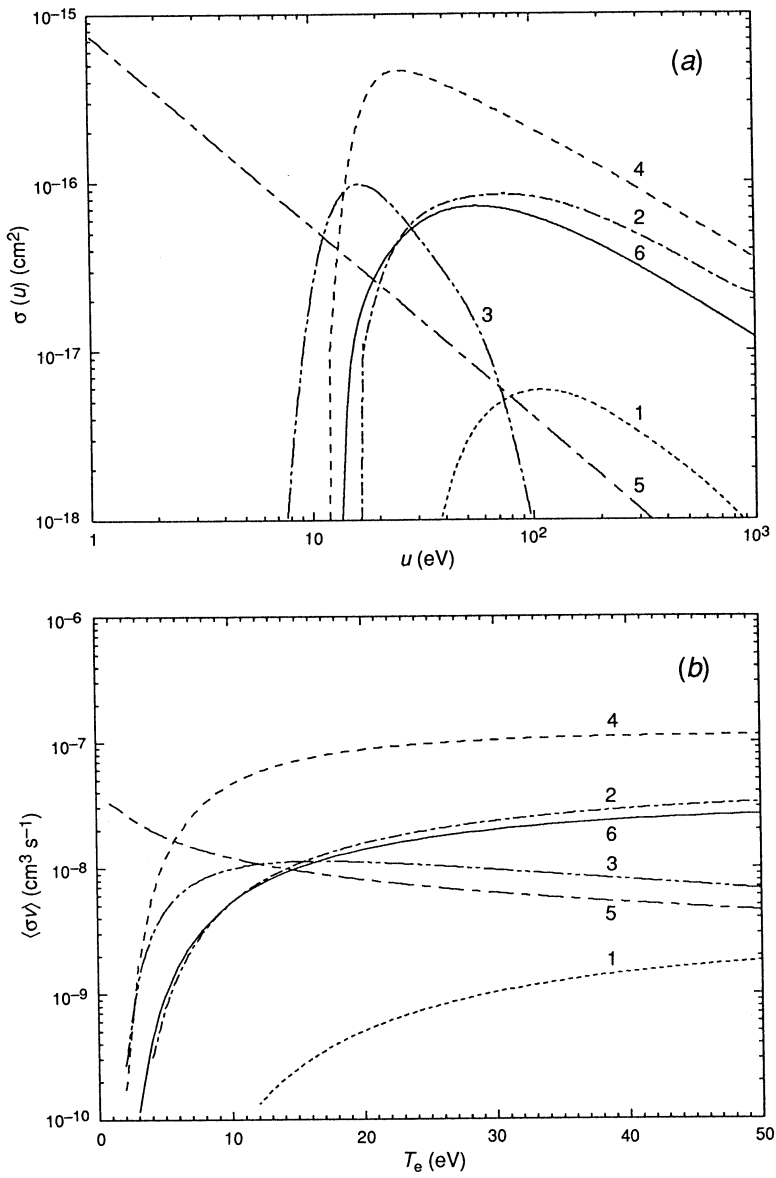

Fig. 1. Hydrogen data showing (*a*) cross sections and (*b*) Maxwellian-averaged reaction rate coefficients:

1 $H_2+e \rightarrow H^+ + H + 2e$
2 $H_2+e \rightarrow H_2^+ + 2e$
3 $H_2+e \rightarrow 2H + e$
4 $H_2^+ + e \rightarrow H^+ + H + e$
5 $H_2^+ + e \rightarrow 2H$
6 $H+e \rightarrow H^+ + 2e$

3. Molecular and Atomic Cross Sections for Hydrogen and Nitrogen

Because of the complexity of the molecular ionisation process (Massey 1969), there is no comprehensive set of cross-section data for all molecular species of

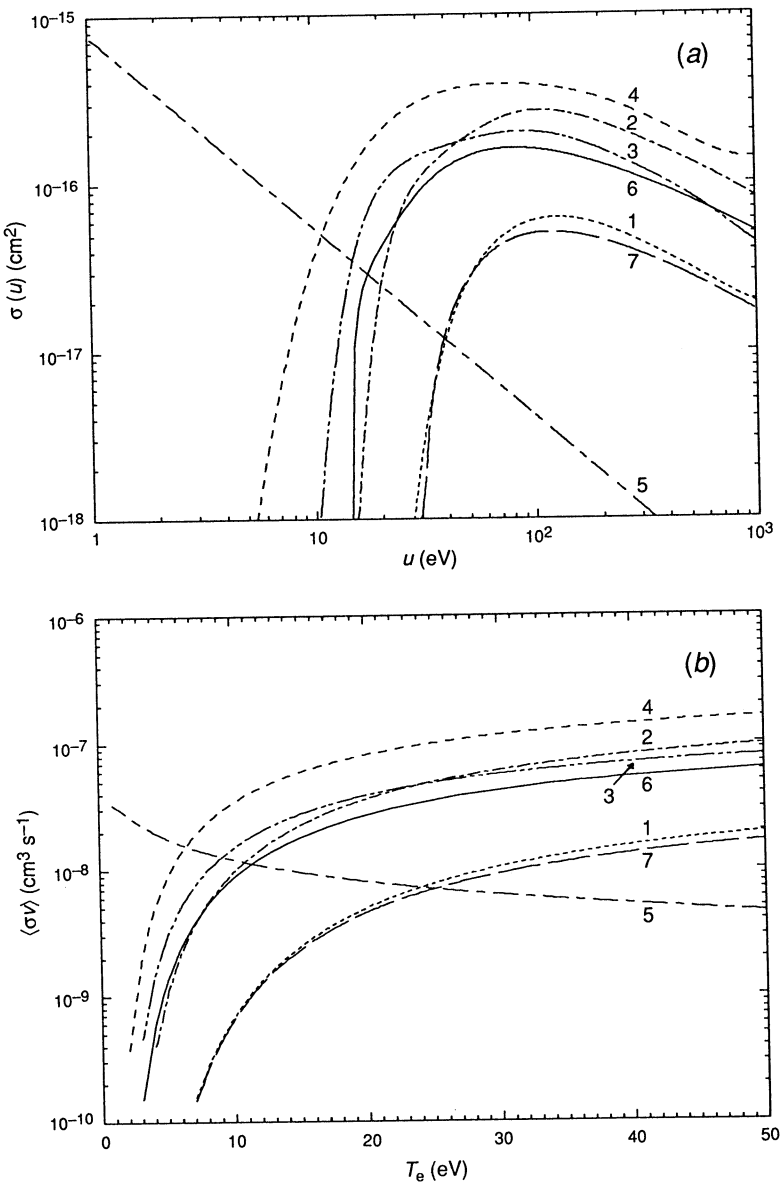

Fig. 2. Nitrogen data showing (*a*) cross sections and (*b*) Maxwellian-averaged reaction rate coefficients:

1 $N_2+e \rightarrow N^+ + N + 2e$
2 $N_2+e \rightarrow N_2^+ + 2e$
3 $N_2+e \rightarrow 2N+e$
4 $N_2^+ + e \rightarrow N^+ + N + e$
5 $N_2^+ + e \rightarrow 2N$
6 $N+e \rightarrow N^+ + 2e$
7 $N^+ + e \rightarrow N^{++} + 2e$

interest. Here we consider only those reactions which are of importance for the determination of the ionisation levels of hydrogen and nitrogen plasmas. The required molecular hydrogen data are available (Jones 1977) but even these

cross sections have uncertainties of up to 50%. The nitrogen data are less complete, and the dissociative recombination cross section has been deduced by comparison with the hydrogen data, with an estimated accuracy of a factor of 2; the results reported here have only a weak dependence on this cross section.

In contrast, the ionisation data for atoms and ions up to nickel are known more accurately (Lennon *et al.* 1986).

Note that we only consider the ionisation of atoms and molecules that are in the ground state. For low density plasmas ($n_e < 10^{12}$ cm^{-3}) the lifetimes of excited states ($\approx 10^{-8}$ s) are sufficiently short that cascade ionisation is negligible (Harrison 1984), and we expect that the density of metastable states is sufficiently low that they do not contribute significantly to the ionisation rate.

The electron ionisation cross-section data for hydrogen and nitrogen molecules, atoms and ions are listed below, with a brief reference to the data source and the order of polynomial that has been used to fit the cross sections over the electron energy range $0 \leq u \leq 1000$ eV.

(a) Molecular Cross Sections

All formulae and least squares (LS) fitted polynomial coefficients are given in the Appendix (see Table 1). The cross sections are plotted in Fig. 1*a* for hydrogen and Fig. 2*a* for nitrogen.

Reaction 1: Dissociative ionisation (D_I)

$$H_2 + e \rightarrow H^+ + H + 2e$$

$$N_2 + e \rightarrow N^+ + N + 2e.$$

Data source: Table C.4.10 of ORNL-5207 by Barnett *et al.* (1977) with polymonial LS fit of seventh degree for both hydrogen and nitrogen.

Reaction 2: Ionisation (I_M)

$$H_2 + e \rightarrow H_2^+ + 2e$$

$$N_2 + e \rightarrow N_2^+ + 2e.$$

Data source: hydrogen: McGowan and Clarke (1978) for $u < 17$ eV and Adamczyk *et al.* (1966) for $u = 17 \rightarrow 1000$ eV with polynomial LS fit of tenth and seventh degrees respectively; nitrogen: Jones (1977) fitted coefficients.

Reaction 3: Dissociation (D)

$$H_2 + e \rightarrow 2H + e$$

$$N_2 + e \rightarrow 2N + e.$$

Data source: hydrogen: formula of Jones (1977); nitrogen: data from Winters (1966) with polynomial LS fit of seventh degree.

Reaction 4: Dissocation of molecular ion (D^+)

$$H_2^+ + e \rightarrow H^+ + H + e$$

$$N_2^+ + e \rightarrow N^+ + N + e.$$

Data source: hydrogen: Peart and Dolder (1972) for $u > 10$ eV with polynomial LS fit of tenth degree; nitrogen: Table C.3.4 of ORNL-5207 by Barnett *et al.* (1977) with polynomial LS fit of seventh degree.

Reaction 5: Dissociative recombination (D_R)

$$H_2^+ + e \rightarrow 2H$$

$$N_2^+ + e \rightarrow 2N.$$

Data source: hydrogen: formula of Jones (1977); nitrogen: complete data available, cross-section set equal to hydrogen cross section since quoted reaction rate coefficients are similar at low energy.

(b) Atomic Cross Sections

Parameters used to evaluate both the atomic cross sections and the reaction rate coefficients are given in the Appendix (see Table 2).

Reaction 6: Atomic ionisation (S_1)

$$H + e \rightarrow H^+ + 2e$$

$$N + e \rightarrow N^+ + 2e.$$

Data source: parameters of Lennon *et al.* (1986).

Reaction 7: Ionisation of singly charged ion (S_2)

$$N^+ + e \rightarrow N^{++} + 2e.$$

Data source: parameters of Lennon *et al.* (1986). Higher level ionisation cross sections can be obtained from Lennon *et al.* (1986) if needed.

4. Reaction Rate Coefficients

As discussed in Section 2, evaluation of the reaction rate coefficients requires the electron energy distribution function to be known. In the absence of diffusion losses, the work of Ferreira and Loureiro (1989) indicates that a Maxwellian distribution is a good approximation to the actual EEDF for the plasmas considered here. We also note that Graves and Jensen (1986) have reported that the assumption of a Maxwelian distribution has led to good predictions of ionisation rates in rf plasmas. However, we expect the EEDF for PI^3 plasmas to be depleted in the tail region because of rapid loss of high energy electrons which are not reflected at the plasmas–wall sheath. Use of a Maxwellian distribution will then overestimate ionisation and dissociation rate coefficients for a given 'temperature'. However, most of the results presented

here tend to depend on ratios of the reaction rate coefficients, which are not so sensitive to changes in the distribution function. Therefore, we approximate the EEDF by a Maxwellian to derive the rate coefficients used in this work. This will not have a qualitive effect on the results presented here, but will lead to a slight underestimate in the prediction of the electron 'temperatures'.

The Maxwellian-averaged reaction rate coefficient is given by

$$\langle \sigma v \rangle = \left(\frac{8e}{\pi m_e T_e^3} \right)^{\frac{1}{2}} \int_0^\infty \sigma(u)\, e^{-u/T_e} u \, du, \tag{1}$$

with u and T_e in eV, and other quantities in SI units.

Using the cross-section library prepared from the data presented in Table 1, the Maxwellian-averaged rate coefficients of molecular hydrogen and molecular nitrogen were evaluated numerically by Simpson's integration, while those of atomic hydrogen and atomic nitrogen were obtained from the Culham formulae and parameters (Lennon *et al.* 1986). The molecular rate coefficients were fitted to the expression (A7); the parameters are given in the Appendix (see Table 3). The reaction rate coefficients are plotted in Fig. 1*b* for hydrogen and in Fig. 2*b* for nitrogen.

5. The Rate Equations

The following notation will be used for an atom species ${}^{Z}A$ forming a diatomic molecule A_2:

x_1 = number density of A_2

x_2 = number density of A_2^+

y_k = number density of $A^{\{k-1\}+}$ $(1 \le k \le Z+1)$,

with reaction rate coefficients defined by

D_1 = dissociative ionisation of A_2 : $A_2 + e \rightarrow A^+ + A + 2e$

I_M = ionisation of A_2 : $A_2 + e \rightarrow A_2^+ + 2e$

D = dissociation of A_2 : $A_2 + e \rightarrow A^+ + A + e$

D^+ = dissociation of A_2^+ : $A_2^+ + e \rightarrow A^+ + A + e$

D_R = dissociative recombination of A_2^+ : $A_2^+ e \rightarrow 2A$

S_k = ionisation of y_k : $A^{\{k-1\}+} + e \rightarrow A^{k+} + 2e$

R_k = recombination of y_k : $A^{\{k-1\}+} + e \rightarrow A^{\{k-2\}+} + h\nu$.

In the derivation of the time-dependent rate equations we have assumed the following:

(1) The densities of all species are spatially uniform. This is a reasonable approximation for the plasmas used in PI^3, as discussed in Section 2.
(2) The mass density of the system is time independent.
(3) The molecular ions A_2^+ have an effective confinement time τ^i before reflecting from the vessel wall as molecules.
(4) The atomic species have confinement times τ_k.
(5) The confinement time of the molecules is infinite since they simply reflect from the vessel wall.
(6) 90% of the atoms and ions reflect from the wall as atoms, 10% reflect as a component of a diatomic molecule (Harrison 1984). The general time-dependent rate equations are as follows:

$$\frac{dx_1}{dt} = -\{(D_I + I_M + D)n_e)\}x_1 + \frac{x_2}{\tau^i} + 0\cdot 05\sum_{k=1}^{Z+1}\frac{y_k}{\tau_k}, \tag{2}$$

$$\frac{dx_2}{dt} = -\left((D^+ + D_R)n_e + \frac{1}{\tau^i}\right)x_2 + (I_M n_e)x_1, \tag{3}$$

$$\frac{dy_1}{dt} = \{(D_I + 2D)n_e\}x_1 + \{(D^+ + 2D_R)n_e\}x_2 - \left(S_1 n_e + \frac{0\cdot 1}{\tau_1}\right)y_1 + \left(R_2 n_e y_2 + 0\cdot 9\sum_{k=2}^{Z+1}\frac{y_k}{\tau_k}\right), \tag{4}$$

$$\frac{dy_2}{dt} = (D_I n_e)x_1 + (D^+ n_e)x_2 + (S_1 n_e)y_1 - \left((S_2 + R_2)n_e + \frac{1}{\tau_2}\right)y_2 + (R_3 n_e)y_3, \tag{5}$$

$$\frac{dy_k}{dt} = (S_{k-1} n_e)y_{k-1} - \left((S_k + R_k)n_e + \frac{1}{\tau_k}\right)y_k + (R_{k+1} n_e)y_{k+1}, \tag{6}$$

for $3 \leq k \leq Z+1$, and

$$n_e = x_2 + \sum_{k=2}^{Z+1}(k-1)y_k. \tag{7}$$

Also, the initial conditions at $t = 0$ are

$$x_1 = X, \quad x_2 = 0, \quad y_k = 0. \tag{8}$$

We restrict our further analysis to plasmas in which wall-induced recombination dominates dielectronic and radiative recombination. This requires

$$R_k n_e \ll 1/\tau_k. \tag{9}$$

Since R_k is typically of order $10^{-9} T_e^{-3/2}$ cm^3 s^{-1} (Post *et al.* 1977), where T_e is the electron temperature in eV, this condition implies

$$n_e \tau_k \ll 10^9 T_e^{3/2} \text{ cm}^{-3}\text{ s}, \tag{10}$$

which is well satisfied for the low density plasmas with short confinement

times that are of interest here. Also, the source terms of the form $(R_{k+1}\, n_e)y_{k+1}$ in (6) are small if (9) is satisfied. Therefore we omit the recombination terms ($R_k = 0$), which simplifies the rate equations and considerably reduces the data requirements. Nevertheless, we are left with a highly nonlinear set of equations to be solved for the time evolution of x_k, y_k and for the final steady-state values.

It is possible to include an equation describing the energy input and loss from the plasma, and this will lead to a time-varying electron temperature. Here we are predominantly interested in the steady-state solutions, so we define T_e to be time independent.

6. Analytic Results

Using a simplified set of steady-state equations ($\mathrm{d}/\mathrm{d}t = 0$) in which all $\tau^i, \tau_k = \tau$ allows the derivation of simple analytic results which are indicative of the behaviour of the more general solutions. The molecular species are ignored ($x_1 = x_2 = 0$) in Sections 6*a* and 6*b*.

(a) Coronal Equilibrium

Retaining the recombination processes R_k and setting $1/\tau = 0$ results in the standard coronal model equilibrium (Griem 1964) in which

$$y_k/y_{k-1} = S_{k-1}/R_k\,. \tag{11}$$

Note that the proportion of each species in this case is independent of the electron density, and the determination of the relative ionisation is a linear problem.

(b) Equilibrium for Small τ

Setting $R_k = 0$ and replacing equation (4) by

$$0 = -(S_1\, n_e + 1/\tau)y_1 + Y/\tau, \tag{12}$$

where

$$Y = \sum_{k=1}^{Z+1} y_k\,, \tag{13}$$

leads to

$$y_1 = \frac{Y}{1 + S_1 n_e \tau} \quad \text{and} \quad \frac{y_k}{y_{k-1}} = \frac{S_{k-1} n_e \tau}{1 + S_k\, n_e \tau}, \quad k > 1. \tag{14}$$

In this case the electron density directly affects the percentage ionisation and, for a given total number density Y, equations (14) and (7) are nonlinear.

An explicit solution can be obtained for atomic hydrogen as only y_1 and y_2 are nonzero, and $n_e = y_2$. This case exhibits a threshold structure as the electron temperature (and the ionisation rate) increases, or as the confinement time increases. Explicitly, we have

$$y_1 = Y \quad \text{and} \quad y_2 = 0 \qquad \text{when} \quad S_1\,\tau < Y^{-1}, \tag{15a}$$

$$y_1 = (S_1\,\tau)^{-1} \quad \text{and} \quad y_2 = Y - (S_1\,\tau)^{-1} \quad \text{when} \quad S_1\,\tau > Y^{-1}. \tag{15b}$$

This simplified model predicts that, in the absence of an exernal source of electrons, ionisation cannot be sustained unless $S_1 \tau > Y^{-1}$. Also, above the threshold, the level of ionisation increases very rapidly as a function of T_e, especially when the threshold temperature T_c is less than 10 eV, as S_1 rises quickly with T_e in this range (see Figs 1 and 2).

(c) Molecular Equilibrium for Small τ

The complete set of rate equations (2)–(7) is too complicated for analytic treatment. However, a reduced set of steady-state equations, which model the most important ionisation processes for hydrogen and nitrogen when n_e is low, can be obtained by setting $D^+ = D_R = S_2 = 0$. By expressing x_2, y_1 and y_2 in terms of x_1, and using the relation $X = x_1 + x_2 + \frac{1}{2}(y_1 + y_2)$, a quadratic equation of the form

$$an_e^2 + bn_e + c = 0 \tag{16}$$

is obtained, where the coefficients are

$$a = [\{I_M \tau + 10(D + D_I)\tau\} S_1 \tau], \tag{17}$$

$$b = [\{S_1 + I_m + 10(D + D_I)\}\tau - S_1 \tau X\{I_M + 20(D + D_I)\}\tau], \tag{18}$$

$$c = [1 - (I_M + D_I)\tau X]. \tag{19}$$

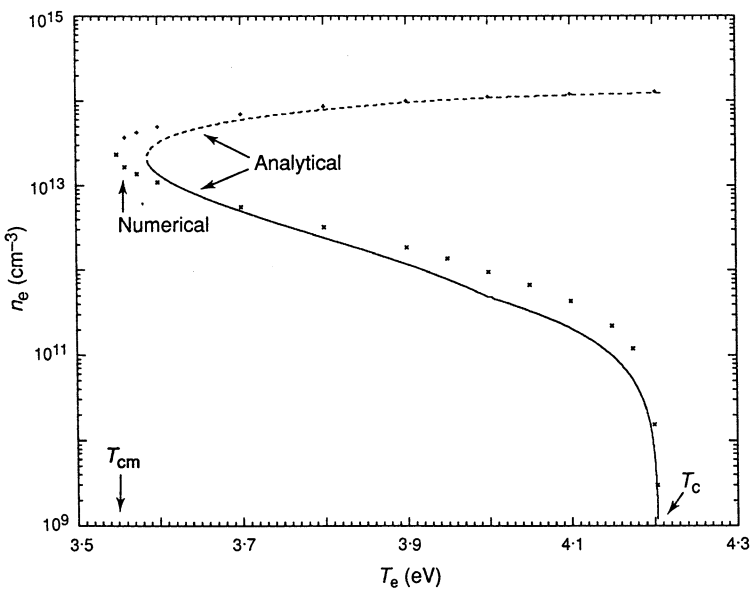

Fig. 3. Steady-state electron density solutions of the rate equations for $X = 10^{14}$ cm^{-3} and $\tau = 20$ μs.

The form of the solution of this equation depends on the relative size of the rate coefficients which determine the sign of b. When $b > 0$, there is a critical temperature T_c derivable from

$$\{I_M(T_c) + D_I(T_c)\}\tau = X^{-1}, \tag{20}$$

below which there is no steady-state ionisation and above which n_e increases rapidly with T_e [similar to the behaviour in (15a) and (15b)]. When $b < 0$, there are two critical temperatures, T_{cm} derivable from the expression $b^2 = 4ac$ and T_c given by (20). In this case, there is no ionisation when $T_e < T_{cm}$, there is a high and a low density solution for n_e when $T_{cm} < T_e < T_c$, and one solution (high density) when $T_e > T_c$. The latter behaviour describes the ionisation of hydrogen and nitrogen, as illustrated for nitrogen in Fig. 3.

7. Solution of the Steady-state Rate Equations

The steady-state ionisation levels of nitrogen have been calculated for a range of electron temperatures using the Maxwellian-averaged rate coefficients. In this and the following sections all $\tau^i, \tau_k = \tau$. Also, as our primary concern here is the study of plasmas with low temperatures, the ionised states higher than y_3 are ignored. Thus the summations are over $k = 1, 2, 3$ only, and $S_3 = 0$.

As $\tau_k = \tau$, the mass conservation condition

$$x_1 + x_2 + \tfrac{1}{2}\sum_{k=1}^{Z+1} y_k = X \tag{21}$$

can be used to eliminate $\Sigma_{k=1}^{Z+1} y_k$ from (2) and (4). The equations (2)–(6) can then be written in matrix form

$$\mathbf{A}.\boldsymbol{x} = \boldsymbol{b}, \tag{22}$$

with $\boldsymbol{x} = \mathrm{col}[x_1, x_2, y_1, y_2, y_3]$. The only nonzero component a_{ij} of $\mathbf{A}$ with $j > i$ is a_{12}. However, equation (22) is nonlinear since the a_{ij} depend on n_e, and

$$n_e = x_2 + y_2 + 2y_3 . \tag{23}$$

For a range of T_e, these equations have been solved interactively as follows:

(i) a value of n_e ($n^{(0)}$) derived from (16) was used to evaluate $\boldsymbol{A}$, and then $\boldsymbol{x}$ was determined;
(ii) a new value of n_e ($n^{(1)}$) was obtained using (23), and
(iii) depending on the size and sign of $(n^{(1)} - n^{(0)})/n(0)$, a new value $n^{(2)}$ was estimated, and the process repeated until satisfactory convergence was obtained.

Now that it is known that the solutions are regular, an automatic root-finding package could be employed.

In Fig. 3 the electron density is shown as a function of T_e for the case of initial molecular density $X = 10^{14}$ cm^{-3} and confinement time $\tau = 20\,\mu$s. In

this case $T_c = 4 \cdot 20$ eV and $T_{cm} = 3 \cdot 55$ eV. For comparison the predictions of equation (16) are also shown (here $T_{cm} = 3 \cdot 59$ eV). It is apparent that the reduced equations give reasonable agreement with the full model. Note that T_c and T_{cm} are quoted to three figure accuracy only to allow comparison of the analytic and numerical results.

It is interesting that, on the lower branch of the solution locus, an increase in n_e is associated with a decrease in T_e. This apparently paradoxical result can be explained as follows. For n_e small, the total ionisation rate is approximately $(I_M x_1 + S_1 y_1) n_e \approx I_M (X + \frac{1}{2} y_1) n_e$, where we have used $S_1 \approx I_M$ and $X \approx x_1 + \frac{1}{2} y_1$.

Equating this to the total recombination rate, which is approximately $(x_2 + y_2)/\tau \; (= n_e/\tau)$, gives $I_m (X + \frac{1}{2} y_1) \tau = 1$. As n_e (and y_1) increase, this relation requires I_M (and therefore T_e) to decrease. We stress that this result only applies when the plasma–wall interaction dominates the recombination process and when the parameter b in (18) is negative.

As our model is only demonstrably valid for low values of n_e, we concentrate on the low density solution branch. The population densities are shown in Fig. 4 as a function of electron temperature. Note that the dominant ion species changes from N_2^+ to N^+ when n_e increases above $3 \cdot 5 \times 10^{11}$ cm^{-3}.

Fig. 5 shows lower branch solutions for the population densities when the initial molecular density is $X = 10^{13}$ cm^{-3}, and $\tau = 20$ μs. For these parameters the agreement between the analytic and the computational results is very good. The effect of lower filling pressure is to increase the value of the electron temperature needed to produce a given electron density, and the critical temperatures are $T_c = 7 \cdot 69$ eV and $T_{cm} = 6 \cdot 69$ eV. In this case the N_2^+ and N^+ ion densities are equal when $n_e = 1 \cdot 1 \times 10^{11}$ cm^{-3}.

It is easily shown using equations (2)–(6) and (16) that, for a sufficiently low electron density ($n_e < 10^{11}$ cm^{-3}), the ratio of N^+ to N_2^+ ions is

$$y_2/x_2 \approx 20 (D/I_M)(n_e/X). \tag{24}$$

For given n_e, this ratio increases as X becomes smaller, although not as rapidly as first expected because there is a simultaneous decrease in (D/I_M) since smaller X implies larger T_e. The ratio also increases as τ is increased, due to (D/I_M) becoming larger. Evaluation of the rate coefficients D and I_M using an EEDF that is depleted in the high energy region compared with a Maxwellian would increase the ratio (D/I_M) and increase the predicted ratio of M^+ to N_2^+ ions. However, following the discussion in Section 2, we do not expect this ratio to change by more than a factor of 2, which is comparable with the uncertainty arising from the cross-section data.

From these results it is apparent that low density plasmas will have temperatures very close to T_c, which lies in the range 3–10 eV for confinement times around 20 μs and filling pressures of 10 mTorr down to 0·1 mTorr. At high filling pressures in particular, the actual electron 'temperature' will depend on how close to Maxwellian is the high energy tail of the electron distribution. These calculations also indicate that low density ($n_e < 10^{11}$ cm^{-3}) nitrogen plasmas created by Maxwellian electrons will have N_2^+ as the predominant ion species. The ratio of N^+ to N_2^+ ions increases with electron density and confinement time, and decreases with filling pressure.

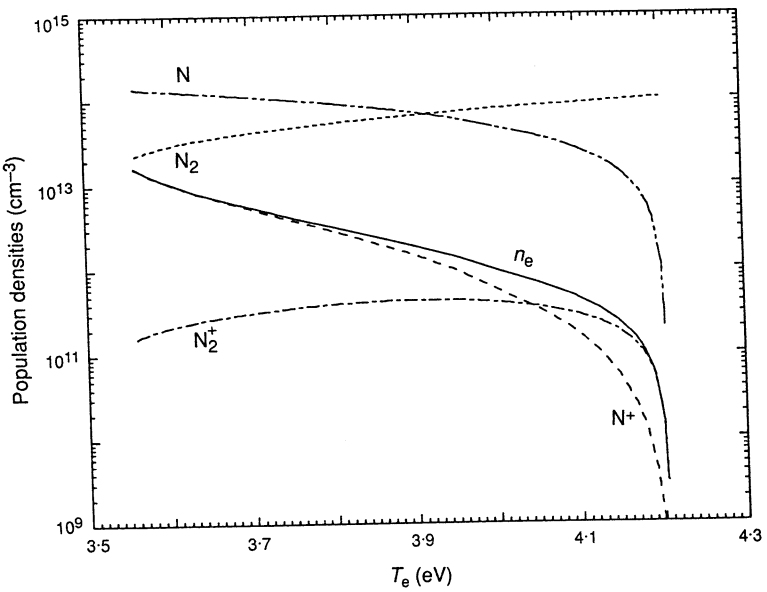

Fig. 4. Population densities for the lower branch of Fig. 3.

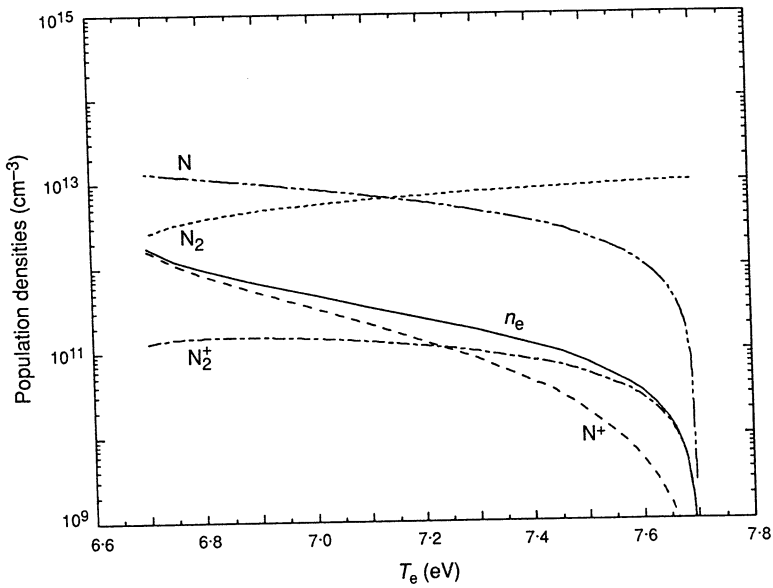

Fig. 5. Population densities for the lower branch solution when $X = 10^{13}$ cm^{-3} and $\tau = 20$ μs.

The sensitivity of the results to the cross-section data can be assessed using the analytic solution in Section 6*c*. Equation (20) and Fig. 2*b* indicates that even a factor of 2 change in the molecular ionisation rate coefficient I_m would alter the temperature T_c only slightly. The temperature T_{cm} depends on

the dissociation rate coefficient D, and the atomic ionisation rate coefficient S_1 which is known accurately. Equation (24) shows that the ratio of N^+ to N_2^+ ions is proportional to D/I_M. Therefore, the largest uncertainty in the results presented here comes from the molecular ionisation and dissociation cross sections. However, a factor of 2 change in I_M or D would not make a qualitative difference to the results.

It is of interest to estimate the power required to maintain the plasma in its ionised state. The major energy loss of relevance for the plasmas considered here comes from radiation during the ionisation process. To a reasonable approximation there is about 100 eV absorbed and radiated per ionisation (Harrison 1984), so the power required to maintain a plasma of density n_e is

$$P \approx 100 e n_e/\tau \quad \mathrm{W\,cm^{-3}}. \tag{25}$$

For a plasma of volume 10^4 cm^3 and confinement time 20 μs, the total power required is $P_T \approx 10^{-8} n_e$ W. In the experimental situation it is the available power which will be the major determinant of n_e.

8. Solution of the Time-dependent Rate Equations

A realistic calculation of time-dependent ionisation requires information concerning the power transfer to the electrons, which will allow determination of the time-dependent plasma 'temperature' and the reaction rate coefficients. We have not modelled this here. However, to obtain some feeling for the rate of approach to the steady state, the time-dependent rate equations were solved under the condition that the electron temperature is fixed. The solutions were found to have some interesting mathematical properties which we briefly describe here. A finite initial value is needed for the electron density to allow evolution of the rate equations. Therefore, over the period $0 \le t \le t_\delta$, we add a small component δn_e to the electron density expression (7). Typically $t_\delta = 10^{-4}$ s and $\delta n_e = 10^6$–10^{10} cm^{-3}. The mathematical package LSODE (Hindmarsh 1980) was used to solve the rate equations.

Calculations have been made for electron temperatures and filling densities in the range $0 < T_e \le 10$ eV and $10^{13} \le X \le 10^{14}$ cm^{-3} respectively, and for confinement times $\tau = 10$, 20 and 40 μs. We find that when $T_e < T_{cm}$ the ionisation induced by the presence of ther 'seed' density δn_e decays away to zero once δn_e is turned off, whereas for $T_e > T_c$ the time-dependent solution always asymptotes to the upper branch value irrespective of the values chosen for t_δ and δn_e.

When $T_{cm} < T_e < T_c$, the time-dependent solution never asymptotes to the lower branch value; initial ionisations just above this equilibrium value approach the upper solution with time, and lower initial ionisations tend to zero. This indicates that the steady-state equilibrium predicted by the lower branch is not asymptotically stable (Hochstadt 1975). The inclusion of another constraint, such as the time-dependent input power, or the electric field at a more fundamental level, is needed to allow the calculation of the evolution to this steady state.

9. Conclusions

A cross-section library for the electron ionisation of hydrogen and nitrogen molecules, atoms and ions has been assembled and used for the derivation of reaction rates assuming a Maxwellian distribution of electron energies. Many of the cross sections have large uncertainties (±50%) and the Maxwellian distribution function used here to derive the rate coefficients is only an approximation, so exact predictions of ionisations levels for a given electron 'temperature' cannot be made. Nevertheless, use of the derived reaction rates allows the identification of the dominant processes that occur during ionisation of plasmas used for plasma immersion ion implantation, and semi-quantitative predictions of the molecular, atomic and ionic densities have been made.

For nitrogen it has been found that, when the dominant recombination mechanism occurs via the plasma–wall interaction, there is a threshold electron temperature below which there is no steady-state ionisation. For a small range of temperatures above this threshold there are two possible ionisation states, but at higher temperatures only the more highly ionised state persists. The threshold temperature decreases slightly as the filling pressure or the confinement time increases.

Solution of the rate equations leads to the prediction that low density nitrogen plasmas (with $n_e < 10^{11}$ cm^{-3}) consist predominantly of N_2^+ ions, and that the electron temperature in these plasmas will be close to the threhold value with only a weak dependence on the plasma density.

Acknowledgment

We thank G. A. Collins and J. Tendys for discussions and information about the plasmas used for PI^3.

References

Adamczyk, B., Boerboom, J. H., Schram, B. L., and Kistemaker, J. (1966). *J. Chem. Phys.* **44**, 4641.

Barnett, C. F., Ray, J. A., Ricci, E., Wilker, M. I., McDaniel, E. W., and Gilbody, H. B. (1977). Atomic data for controlled fusion research. Oak Ridge Nat. Lab. Rep. ORNL-5207 (Vol. II of ORNL-5206).

Coburn, J. W., and Winters, H. F. (1983). *Ann. Rev. Mater. Sci.* **13**, 91.

Conrad, J. R., Radtke, J. L., Dodd, R. A., Worzala, F. J., and Tran, N. C. (1987). *J. Appl. Phys.* **62**, 4591.

Donnelly, I. J., Rose, E. K., and Cook, J. L. (1987). *Aust. J. Phys.* **40**, 393.

Ferreira, C. M., and Loureiro, J. (1989). *J. Phys.* D **22**, 76.

Graves, D. B., and Jensen, K. F. (1986). *IEEE Trans. Plasma Sci.* **PS-14**, 78.

Griem, H. R. (1964). 'Plasma Spectroscopy', pp. 166–7. (McGraw–Hill: New York).

Harrison, M. F. A. (1984). *In* 'Applied Atomic Collison Physics', Vol. 2 (Eds H. S. W. Massey *et al.*) (North–Holland: Amsterdam).

Hess, D. W. (1986). *Ann. Rev. Mater. Sci.* **16**, 163.

Hindmarsh, C. (1980). LSODE—Livermore solver for ordinary differential equations. National Energy Software Center Note 81–70. Argonne Nat. Lab.

Hochstadt, H. (1975). 'Differential Equations—A Modern Approach' (Dover: New York).

Jones, E. M. (1977). Atomic collision processes in plasma physics experiments: Analytic expressions for selected cross-sections and Maxwellian rate coefficients II. Culham Lab. Rep. CLM-R175.

Korhonen, A. S., Molarious, J. M., and Sulonen, M. S. (1988). *Surf. Engineering* **4**, 44.

Kushner, M. J. (1983). *J. Appl. Phys.* **54**, 4958.

Lennon, M. A., Bell, K. L., Gilbody, H. B., Hughes, J. G., Kingston, A. E., Murray, M. J., and Smith, F. J. (1986). Atomic and molecular data for fusion, Part 2: Recommended cross-sections and rates for electron ionisation of light atoms and ions: Fluorine to nickel. Culham Lab. Rep. CLM-R175.
McGowan, J. W., and Clarke, E. M. (1968). *Phys. Rev.* **167**, 43.
Massey, H. S. W. (1969). 'Electronic and Ionic Impact Phenomena', Vol. 2 (Oxford University Press).
Peart, B., and Dolder, K. T. (1972). *J. Phys.* **B 5**, 860.
Post, D. E., Jensen, R. V., Tarter, C. B., Grasberger, W. H., and Lokke, W. A. (1977). *At. Data Nucl. Data Tables* **20**, 397.
Tendys, J., Donnelly, I. J., Kenny, M. J., and Pollock, J. T. A. (1988). *Appl. Phys. Lett.* **53**, 2143.
Thornton, J. A. (1982). *In* 'Deposition Technologies for Films and Coatings' (Ed. R. F. Bunshah), p.19 (Noyes Publications: New Jersey).
Winters, H. F. (1966). *J. Chem. Phys.* **44**, 1472.

Appendix: Parameters and Formulae for the Evaluation of Molecular and Atomic Cross Sections and Reaction Rate Coefficients

Molecular Cross Sections (see Table 1)

The experimental cross-section data were least squares fitted to polynomials of the form

$$\ln\{\sigma(u)\} = \sum_{k=0}^{m} a_k (\ln u)^k \tag{A1}$$

for all reactions except reaction 3 for hydrogen and reaction 5 for both hydrogen and nitrogen, which are given by the following formulae respectively:

$$\sigma(u) = a_0 \exp\{a_1(1 - a_2/u)^2\}\{1 + a_3(u/10)^6\}^{-1}, \tag{A2}$$

$$\sigma(u) = a_0 u^{a_1}. \tag{A3}$$

The coefficients in Table 1 contain the number of significant figures necessary to fit the data to within a few per cent.

Here the following units are used: σ (cm^2), $\langle\sigma v\rangle$ (cm^3 s^{-1}) and u, T_e, I (eV). Most of these cross sections have threshold energies, which are given by the lower limits on u.

Atomic Ionisation Cross Sections of Hydrogen and Nitrogen (see Table 2)

Lennon *et al.* (1986) have fitted the recommended experimental cross sections to the formula

$$\sigma(u) = \left(A \ln(u/I) + \sum_{i=1}^{m} B_i (1 - I/u)^i\right)/Iu, \tag{A4}$$

and the Maxwellian-averaged rate coefficients to

$$\langle\sigma v\rangle = \exp(-I/T_e)\,(T_e/I)^{\frac{1}{2}} \sum_{n=0}^{5} a_n \{\log_{10}(T_e/I)\}^n, \tag{A5}$$

for $I/10 \leq T_e \leq 10I$, and

Table 1. Parameters for evaluation of the molecular cross sections

	Hydrogen		Nitrogen
	$H_2+e \rightarrow H^+ + H + 2e$		$N_2+e \rightarrow N^+ + N + 2e$
	$u > 20$ eV		$u > 24.3$ eV
a_0	-4.0332773×10^{3}		-1.9037403×10^{3}
a_1	5.3046146×10^{3}		2.4042565×10^{3}
a_2	-3.0149980×10^{3}		-1.3316545×10^{3}
a_3	9.4911209×10^{2}		4.1000112×10^{2}
a_4	-1.7850702×10^{2}		-7.5624902×10^{1}
a_5	2.0042070×10^{1}		8.3445534×10^{0}
a_6	-1.2432159×10^{0}		-5.0959915×10^{-1}
a_7	3.2858178×10^{-2}		1.3282128×10^{-2}
	$H_2+e \rightarrow H_2^+ + 2e$		$N_2+e \rightarrow N_2^+ + 2e$
	$15.3 < u \leq 17$ eV	$17 \leq u \leq 1000$ eV	$u > 15.6$ eV
a_0	7.905779677×10^{5}	-8.76479000×10^{2}	-7.0402111×10^{3}
a_1	-1.414957639×10^{6}	1.1944600×10^{3}	1.2929580×10^{4}
a_2	2.921861411×10^{5}	-7.2486146×10^{2}	-1.0707225×10^{4}
a_3	1.590111203×10^{5}	2.4276337×10^{2}	5.2558480×10^{3}
a_4	2.641947693×10^{4}	-4.8399137×10^{1}	-1.7030313×10^{3}
a_5	-1.029228430×10^{4}	5.7404643×10^{0}	3.8386812×10^{2}
a_6	-1.472615646×10^{4}	-3.7503782×10^{1}	-6.1751117×10^{1}
a_7	1.320556583×10^{3}	1.0414050×10^{-2}	7.1479523×10^{0}
a_8	5.303386425×10^{1}		-5.9134110×10^{-1}
a_9	6.374322653×10^{2}		3.4124824×10^{-2}
a_{10}	-1.381337136×10^{2}		-1.3049737×10^{-3}
a_{11}			2.9716990×10^{-5}
a_{12}			-3.0500239×10^{-7}
	$H_2+e \rightarrow 2H+e$ (A2)		$N_2+e \rightarrow 2N+e$
	$u > 3$ eV		$u > 9.76$ eV
a_0	9.7×10^{-17}		-6.9745122×10^{2}
a_1	-3.4×10^{0}		9.7348239×10^{2}
a_2	16.5×10^{0}		-6.0801230×10^{2}
a_3	1.0×10^{-5}		2.0841938×10^{2}
a_4			-4.2305572×10^{1}
a_5			5.0844690×10^{0}
a_6			-3.3518666×10^{-1}
a_7			9.3564824×10^{-3}
	$H_2^+ + e \rightarrow H^+ + H + e$		$N_2^+ + e \rightarrow N^+ + N + e$
	$u > 11.5$ eV		$u > 8.7$ eV
a_0	-2.8517997×10^{3}		-7.6121058×10^{1}
a_1	4.8273269×10^{3}		3.9053996×10^{1}
a_2	-3.5113259×10^{3}		-1.5447728×10^{1}
a_3	1.3763026×10^{3}		3.2706880×10^{0}
a_4	-2.9237054×10^{2}		-4.2131611×10^{-1}
a_5	2.1786055×10^{1}		3.9683601×10^{-2}
a_6	4.7620135×10^{0}		-3.1310304×10^{-3}
a_7	-1.5203316×10^{0}		1.3884698×10^{-4}
a_8	1.8684905×10^{1}		
a_9	-1.1449991×10^{2}		
a_{10}	2.8867096×10^{-4}		
	$H_2^+ + e \rightarrow 2H$ (A3)		$N_2^+ + e \rightarrow 2N$ (A3)
	$u > 0.1$ eV		$u > 0.3$ eV
a_0	7.6×10^{16}		7.6×10^{-16}
a_1	-1.14×10^{0}		-1.14×10^{0}

Table 2. Parameters of equations (A4), (A5) and (A6)

	m	I	A	B_1	B_2	B_3	B_4
H	4	13·6	1·845E–14	–1·860E–15	1·230E–14	–1·900E–14	9·530E–14
N	3	14·5	2·265E–13	–1·710E–13	–2·322E–13	1·732E–13	
N^+	4	29·6	1·076E–13	–8·290E–14	8·720E–14	–1·620E–14	1·533E–13
	a_0	a_1	a_2	a_3	a_4	a_5	
H	2·3742E–8	–3·6867E–9	–1·0366E–8	–3·8010E–9	3·4159E–9	1·6834E–9	
N	4·6209E–8	9·2265E–9	–1·2092E–8	–2·4852E–8	5·1361E–9	8·3068E–9	
N^+	2·4382E–8	–2·2167E–9	–1·4813E–8	–4·4241E–10	4·5235E–9	1·7883E–10	
	α	β_0	β_1	β_2			
H	2·4617E–8	9·5987–8	–9·2464E–7	3·9974E–6			
N	2·7367E–7	–4·2976E–7	9·8343E–7	–9·5697E–7			
N^+	4·4713E–8	3·0447E–8	–5·2724E–7	2·4876E–6			

Table 3. Parameters for the evaluation of the reaction rate coefficients for molecular hydrogen and nitrogen

	Hydrogen	Nitrogen
	$H_2+e \rightarrow H^+ + H + 2e$	$N_2+e \rightarrow N^+ + N + 2e$
a_0	$-4·8140\times10^{1}$	$-4·5984\times10^{1}$
a_1	$2·3597\times10^{1}$	$2·5947\times10^{1}$
a_2	$-9·3122\times10^{0}$	$-1·2330\times10^{1}$
a_3	$2·2558\times10^{0}$	$3·7330\times10^{0}$
a_4	$-3·2168\times10^{-1}$	$-6·4205\times10^{-1}$
a_5	$2·0195\times10^{-2}$	$4·6175\times10^{-2}$
	$H_2+e \rightarrow H_2^+ + 2e$	$N_2+e \rightarrow N_2^+ + 2e$
a_0	$-3·4430\times10^{1}$	$-3·4697\times10^{1}$
a_1	$1·6038\times10^{1}$	$1·6160\times10^{1}$
a_2	$-7·2349\times10^{0}$	$-6·8302\times10^{0}$
a_3	$1·9602\times10^{0}$	$1·7310\times10^{0}$
a_4	$-2·9796\times10^{-1}$	$-2·4254\times10^{-1}$
a_5	$1·9217\times10^{-2}$	$1·4202\times10^{-2}$
	$H_2+e \rightarrow 2H+e$	$N_2+e \rightarrow 2N+e$
a_0	$-2·6564\times10^{1}$	$-2·9574\times10^{1}$
a_1	$8·6277\times10^{0}$	$1·1029\times10^{1}$
a_2	$-3·5440\times10^{0}$	$-4·2516\times10^{0}$
a_3	$7·8138\times10^{-1}$	$9·3719\times10^{-1}$
a_4	$-1·0189\times10^{-1}$	$-1·0929\times10^{-1}$
a_3	$5·7942\times10^{-3}$	$5·0481\times10^{-3}$
	$H_2^+ + e \rightarrow H^+ + H + e$	$N_2^+ + e \rightarrow N^+ + N + e$
a_0	$-2·8984\times10^{1}$	$-2·6139\times10^{1}$
a_1	$1·2450\times10^{1}$	$8·3516\times10^{0}$
a_2	$-5·2089\times10^{0}$	$-3·4055\times10^{0}$
a_3	$1·2335\times10^{0}$	$9·2035\times10^{-1}$
a_4	$-1·6582\times10^{-1}$	$-1·4664\times10^{-1}$
a_5	$9·8020\times10^{-3}$	$1·0006\times10^{-2}$
	$H_2^+ + e \rightarrow 2H$	$N_2^+ + e \rightarrow 2N$
a_0	$-1·7226\times10^{1}$	$-1·7226\times10^{1}$
a_1	$-1·0527\times10^{-1}$	$-1·0527\times10^{-1}$
a_2	$-2·7138\times10^{-1}$	$-2·7138\times10^{-1}$
a_3	$8·1508\times10^{-2}$	$8·1583\times10^{-2}$
a_4	$-1·3469\times10^{-2}$	$-1·3649\times10^{-2}$
a_5	$9·2946\times10^{-4}$	$9·2946\times10^{-4}$

$$\langle \sigma v \rangle = (T_e/I)^{-\frac{1}{2}} \left(\alpha \ln(T_e/I) + \sum_{n=0}^{2} \beta_n (T_e/I)^{-n} \right), \tag{A6}$$

for $T_e > 10I$.

Reaction Rate Coefficients for H_2 and N_2 (see Table 3)

Maxwellian-averaged data were least squares fitted to polynomials of the form

$$\ln\langle \sigma v \rangle = \sum_{k=0}^{m} a_k (\ln T_e)^k , \tag{A7}$$

with $m = 5$ for all reactions.

Manuscript received 24 April, accepted 2 November 1989